



New insights on the molecular features and electrophysiological properties of dinotefuran, imidacloprid and acetamiprid neonicotinoid insecticides

Jean-Yves Le Questel^{a,*}, Jérôme Graton^a, José P. Cerón-Carrasco^a, Denis Jacquemin^a
Aurélien Planchat^a, Steeve H. Thany^{b,*}

^a Université de Nantes, CEISAM UMR 6230, UFR des Sciences et des Techniques, 2 rue de la Houssinière, BP 92208, Nantes F-44000, France

^b Université d'Angers, Récepteurs et Canaux Ioniques Membranaires, UPRES EA 2647, USC INRA 2023, UFR Sciences, 2 boulevard Lavoisier, 49045 Angers cedex, France

ARTICLE INFO

Article history:

Received 20 July 2011

Revised 6 October 2011

Accepted 7 October 2011

Available online 20 October 2011

Keywords:

Neonicotinoids

Nicotinic acetylcholine receptor

Quantum chemistry calculations

Conformational features

Hydrogen-bonding

ABSTRACT

Structural features and hydrogen-bond interactions of dinotefuran (DIN), imidacloprid (IMI) and acetamiprid (ACE) have been investigated experimentally through analyses of new crystal structures and observations in structural databases, as well as by Density Functional Theory quantum chemical calculations. Several conformations are observed experimentally in the solid state, highlighting the large flexibility of these compounds. This feature is confirmed by the theoretical calculations in the gas phase, the numerous and different energetic minima of the three neonicotinoids being located within a 10 kJ/mol range. Comparisons of the observed and simulated data sheds light on the hydrogen-bond (HB) strength of the functional group at the tip of the electronegative fragment of each pharmacophore (NO₂ for DIN and IMI and C≡N for ACE). This effect originates in the 'push-pull' nature of these fragments and the related extensive electron delocalization. Molecular electrostatic potential calculations provide a ranking of the two fragments of the three neonicotinoid in terms of HB strength. Thus, the NO₂ group of DIN is the strongest HB acceptor of the electronegative fragment, closely followed by the cyano group of ACE. These two groups are significantly more potent than the NO₂ group of IMI. With respect to the other fragments of the three neonicotinoids, the nitrogen atom of the pyridine of IMI and ACE are stronger HB acceptors than the oxygen atom of the furanyl moiety of DIN. Finally, compared to electrophysiological studies obtained from cockroach synaptic and extrasynaptic receptors, DIN appears more effective than IMI and ACE because it strongly increases dose-dependently the ganglionic depolarisation and the currents amplitudes. These data suggest that DIN, IMI and ACE belong to two subgroups which act differently as agonists of insect nicotinic receptors.

© 2011 Elsevier Ltd. All rights reserved.

1. Introduction

Neonicotinoids are the fastest growing class of insecticides, used worldwide since the introduction of carbamates and pyrethroids¹ acting as full or partial agonists of insect nicotinic acetylcholine receptors (nAChRs).² Recently, promising new representatives of this class of compounds have been designed. Indeed, the fixation of the nitro group in a *cis* configuration in several types of neonicotinoids have been shown to lead to compounds having distinct biological activities and behaving as promising tools for the elucidation of the pharmacology and nature of the neonicotinoid binding sites.^{3–5} Neonicotinoids include five-membered ring derivatives (imidacloprid, thiacloprid), six-membered ring compounds (thiamethoxam) as well as noncyclic structures (nitenpyram, acetamiprid, clothianidin, dinotefuran) used against a broad spectrum of pests.⁶ The chemical diversity of neonicotinoids can be illustrated

by imidacloprid (IMI), acetamiprid (ACE) and dinotefuran (DIN) (Fig. 1). IMI, the forerunner of neonicotinoids, remains the most important representative of these compounds,⁷ and is constituted of chloropyridinylmethyl (CPM) and *N*-nitroimine substituents. ACE is formed with CPM and *N*-cyanoimine groups and DIN contains tetrahydrofurylmethyl (TFM) and *N*-nitroimine moieties. These three compounds are part of the seven neonicotinoids currently market-available and extensively used for crop protection.^{8,9} Owing to the difficulty to express insect nAChRs in heterologous systems, the first attempts for understanding neonicotinoid-nAChR subtype interactions involved site-directed mutagenesis or chimeragenesis that allowed to evaluate the role of specific subunit(s), region(s) or amino acid(s) on the pharmacological response.^{10–13} The more recent structural biology analysis based on high-resolution X-ray crystallography reveals (i) orientations of functional amino acids in the ligand-bound state, (ii) conformational rearrangements of the protein upon ligand occupation and (iii) gives insights regarding ligand–protein interactions.¹⁴ Indeed, the determination of various X-ray crystal structures of the free and ligand bound molluscan ACh-binding proteins (AChBPs), which are soluble protein

* Corresponding authors.

E-mail addresses: Jean-Yves.Le-Questel@univ-nantes.fr (J.-Y. Le Questel), steeve.thany@univ-angers.fr (S.H. Thany).

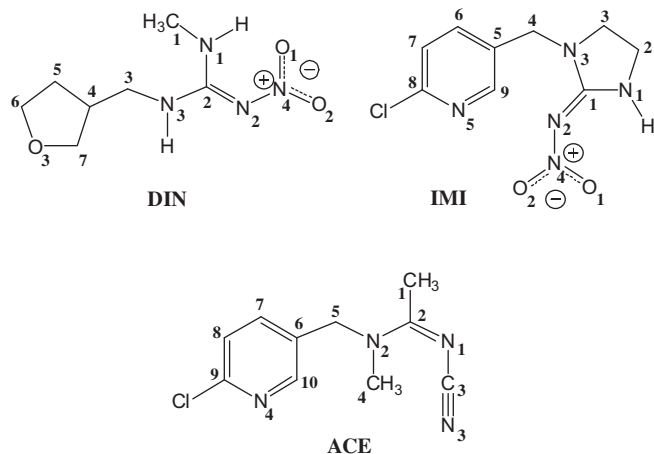


Figure 1. Chemical structures of IMI, ACE and DIN.

homologues of the extracellular domains (ECDs) of *nAChRs*, have provided an atomic picture of the *nAChRs* structure as well as common concepts for neonicotinoid-ECD interactions.^{15–17} These structural studies have pointed out the key role of hydrogen-bond (HB) interactions for binding of neonicotinoids to *nAChRs*, for both moieties of the ligands.^{15–17} In the binding process, the contribution of π – π stacking interactions between the planar conjugated moiety of the neonicotinoid ligands and aromatic residues of the *nAChRs*, in particular the key Trp residue, has been pointed out, both from X-ray crystallographic studies^{17,18} and quantum chemical investigations on model systems.⁵ HB interactions are important for the selectivity of binding of neonicotinoids to *nAChRs* but such π – π interactions, by nature dispersive, and more difficult to evaluate, play a role in the thermodynamics of the binding process. Despite this recognised importance of HB interactions, the structure–activity relationship (SAR) regarding the hydrogen-bonding abilities of neonicotinoid substituents is not fully understood and, to the best of our knowledge, remains to be investigated in detail. Only one recent study from Ohno and co-workers¹⁹ focused on the water-mediated ligand–protein interactions of 2-nitroimidazoimidazolidine analogues. More precisely, the hydrogen-bonding ability of neonicotinoid probes with suitably positioned HB acceptor substituents potentially able to interact with the water molecule bridging the ligand to AChBP binding site residues has been investigated. Such studies pave the way for the design of new neonicotinoid with novel substituents.

In the present work, we have selected DIN, IMI and ACE owing to their distinct chemical features, in order to throw light on their structural and HB properties through experimental (X-ray crystallography) and theoretical (Density Functional Theory) studies. We completed these physicochemical investigations by electrophysiological studies using mannitol-gap and patch clamp techniques to evaluate and compare their agonist actions on both cockroach postsynaptic and extrasynaptic *nAChRs*. In a first step, the crystal structures of DIN, IMI and ACE and the HB interactions observed in the solid state for the three neonicotinoids are described. We have identified the minima of DIN and ACE that appear the closest to the conformation of IMI observed in the binding site of *Aplysia* AChBP. The computation of quantum descriptors based on the molecular electrostatic potential (MEP) allowed to pinpoint significant differences in terms of HB abilities of the three compounds. In a second step, electrophysiological studies throw light on the difference of biological effects of the three neonicotinoids. Thus, we found that all three of them act as agonists of postsynaptic *nAChRs* while at extrasynaptic *nAChRs* IMI and ACE have lower affinities compared to DIN.

2. Material and methods

2.1. X-ray diffraction

2.1.1. Dinotefuran

Crystals of DIN were grown by slow evaporation of an ethanol/water (50:50) solution at room temperature. X-ray data: $C_7H_{14}N_4O_3$, $M_w = 202.22$, colourless block, monoclinic, $P2_1/c$, $a = 5.5250(4)$ Å, $b = 17.1231(14)$ Å, $c = 10.1868(6)$ Å, $\beta = 90.858(8)^\circ$, $V = 963.12(12)$ Å³, $Z = 4$, $D_x = 1.394$ g cm^{−3}, $\mu = 0.11$ mm^{−1}, $F(000) = 432$, 20319 reflections were measured on a Nonius-Kappa CCD diffractometer (graphite monochromator, $\lambda = 0.71073$ Å) up to a resolution of $(\sin \theta/\lambda)_{\max} = 0.67$ Å^{−1} at 293 K, $R_{\text{int}} = 0.063$. Numbers of reflections ($I \geq 2\sigma(I)$) = 2415, $R = 0.0684$, $wR = 0.149$, $R(\text{all}) = 0.1018$, $wR(\text{all}) = 0.1710$. The structure was solved using the charge flipping algorithm²⁰ implemented in the Superflip program²¹ and refined with the JANA2006 program²² against F^2 for all reflections. Nonhydrogen atoms were refined with anisotropic displacement parameters. All H atoms were introduced in geometrically optimised positions and refined with a riding model.

2.1.2. Imidacloprid

Crystals of IMI were grown by slow evaporation of an ethanol/water (50:50) solution at room temperature. X-ray data: $C_9H_{10}N_5O_2Cl$, $M_w = 255.7$, colourless plate, monoclinic, $P2_1/n$, $a = 12.3669(14)$ Å, $b = 9.5359(8)$ Å, $c = 18.842(3)$ Å, $\beta = 102.647(12)^\circ$, $V = 2168.1(5)$ Å³, $Z = 8$, $D_x = 1.566$ g cm^{−3}, $\mu = 0.351$ mm^{−1}, $F(000) = 1056$, 40581 reflections were measured on a Nonius-Kappa CCD diffractometer (graphite monochromator, $\lambda = 0.71073$ Å) up to a resolution of $(\sin \theta/\lambda)_{\max} = 0.72$ Å^{−1} and an Oxford cryostream cooler for the low temperature achievement (120 K), $R_{\text{int}} = 0.068$. Numbers of reflections ($I \geq 2\sigma(I)$) = 6653, $R = 0.0680$, $wR = 0.120$, $R(\text{all}) = 0.1295$, $wR(\text{all}) = 0.1436$. The structure was solved using the charge flipping algorithm²⁰ implemented in the Superflip program²¹ and refined with JANA2006 program²² against F^2 for all reflections. Nonhydrogen atoms were refined with anisotropic displacement parameters. All H atoms were introduced in geometrically optimised positions and refined with a riding model except for nitrogen H atoms in imidazolidine ring, which positions were determined by difference Fourier.

CCDC 827010 and CCDC 835289 contain respectively the supplementary crystallographic data for dinotefuran and imidacloprid crystal structures described in this paper. These data can be obtained free of charge from the Cambridge Crystallographic Data Centre via www.ccdc.cam.ac.uk/data_request/cif.

The analyses of the hydrogen bonding interactions in the crystal structures of IMI and ACE found in the Cambridge Structural Database (CSD)²³ together with the ones of DIN and IMI resolved in the present work have been conducted with the Mercury program (version 2.4).²⁴ To reach a better accuracy on the HB parameters, the X–H distances were normalised to their values measured by neutron diffraction (C–H, N–H and O–H distances of 1.083, 1.009 and 0.983 Å, respectively). The overlays of these structures were carried out using the Pymol program.²⁵

2.2. Quantum chemistry calculations

Theoretical calculations were performed using GAUSSIAN 09²⁶ and JAGUAR²⁷ programs.

2.2.1. Conformational study

Owing to their excellent performance-to-cost ratio, DFT methods constitute very appealing approaches. In the present work, we selected the MPWB1K functional²⁸ which had proven to surpass other functionals for energy-barrier prediction and

nonbonded interactions²⁸ associated to the 6-31+G(d,p) atomic basis set to perform our conformational investigations in the gas phase. The harmonic frequencies were computed analytically in order to characterise the stationary points. It was recognised that intramolecular basis set superposition error (BSSE) impacts significantly the relative energies of conformations with different degrees of compactness.²⁹ Beside dispersion effects, due to interactions between aromatic fragments, weak intramolecular hydrogen-bonding interactions were also involved in these theory-experiment discrepancies.^{29,30} The need for accurate theoretical estimations of conformational energies led to the design of methods less BSSE-prone. In that framework, the local MP2 (LMP2) methodology was highly efficient in correcting the errors related to these interactions.^{31,32} Because DIN and IMI showed stable conformations including intramolecular interactions, single-point calculations were carried out at the LMP2/aug-cc-pVTZ(-f)//MPWB1K/6-31+G(d,p) level of theory. Estimated ZPVE and thermodynamic corrections derived from the MPWB1K/6-31+G(d,p) harmonic frequencies were used such that our method can be briefly described as LMP2/aug-cc-pVTZ(-f)//MPWB1K/6-31+G(d,p) level. The relative population of each conformer was evaluated from the Gibbs energies considering a Boltzmann distribution according to Eq. (1):

$$P_i = \frac{e^{-\Delta G_i/RT}}{\sum_{i=1}^n e^{-\Delta G_i/RT}} \quad (1)$$

2.2.2. HB properties characterisation

Since the original works of Murray and Politzer,^{33–36} it has been consistently demonstrated that HB basicity and the minimum electrostatic potential were rather well correlated, owing to the mainly electrostatic character of the HB interaction. The absolute minimum values of the electrostatic potential, V_{\min} , located on each HBA site were calculated using the HS95 program.^{37,38} Because DIN, IMI, and ACE can all be found under several conformations, they may present contrasted HB basicities. Theoretical calculations must therefore take into account the flexibility of the monomer to gain more realistic insights. In recent works, we have shown that a weighting of the electrostatic potentials or interaction energies by relative Boltzmann populations provided satisfactory descriptions of the experimental HB basicities.^{39–41} HB acidity can be characterised as well by an electrostatic descriptor such as $V_{s,\max}$ or $V_{\alpha}(r)$ a more accurate descriptor recently recommended by Kenny.⁴² The $V_{\alpha}(r)$ descriptor was defined as the molecular electrostatic potential calculated at a distance $r = 0.55 \text{ \AA}$ from the donor hydrogen atom along the axis defined by the vector formed by the hydrogen and the atom to which it was bonded. The $V_{\alpha}(r)$ values were calculated on the NH hydrogen atom of DIN and IMI for the characterisation of their potential HB acidity. These two compounds are also likely to give intramolecular interactions between their NH and NO_2 groups. Those interactions were characterised from electron densities computed at the critical points of the corresponding HB, within the framework of Atoms in Molecules (AIM) theory^{43,44} as implemented in the AIM2000 program.⁴⁵

2.3. Electrophysiological studies

2.3.1. Mannitol-gap recordings

Experiments were performed using adult male cockroaches *Periplaneta americana* reared at room temperature 29°C on 12 h: 12 h light dark cycle. They were dissected and opened along the longitudinal dorsal-median line. A fine pair of forceps was carefully used to remove the alimentary canal and overlying muscle and tracheae. The abdominal nerve cord, one cercus and the correspond-

ing cercal nerve XI were isolated and immediately flooded with saline of the following composition (in mM): NaCl, 208; KCl, 3.1; CaCl_2 , 5.4; NaHCO_3 , 2; Sucrose, 26; pH 7.4.⁴⁶ The preparation was then removed and transferred to the recording chamber and continuously superfused with saline and mannitol solution (87 g/L).⁴⁷ Ganglionic depolarisations induced by DIN, IMI and ACE were recorded using an Axopatch 200B amplifier (Axon instruments, Foster City, CA), connected to a computer with the pClamp software control (pClamp 10.0, Axon Instruments). DIN, IMI and ACE and were applied during 3 min⁴⁶ with a Micropump fast perfusion (Harvard Apparatus) that produced a constant solution exchange (500 $\mu\text{L}/\text{min}$). The dose–response curve was derived from the fitted curve following Eq. (2):

$$Y = Vd_{\min} + (Vd_{\max} - Vd_{\min}) / (1 + 10^{(\log EC_{50} - X)H}) \quad (2)$$

where Y is the normalised response, Vd_{\max} and Vd_{\min} are the maximum and minimum responses, H is the Hill slope, EC_{50} is the concentration giving half the maximum response and X is the logarithm of the compound concentration.

2.3.2. Patch-clamp recordings

Recordings were performed on adult dorsal unpaired median (DUM) neuron cell bodies isolated from the sixth abdominal ganglion, following enzymatic treatment and mechanical dissociation as previously described.^{48,49} DIN, IMI and ACE-induced currents were recorded using the patch-clamp technique in the whole-cell recording configuration under voltage-clamp mode with an axopatch 200B (Patch-clamp amplifier, Axon Instruments, Foster City, CA). Signals were digitized and acquired using a MiniDigidata 1440 analogue-digital converter (Axon Instruments) and axoscope 10.2 software (Axon Instruments). The Petridish containing isolated cell bodies was placed onto the inverted microscope (CK2: Olympus), and continuously bathed with the standard extracellular solution (in mM: NaCl 200, KCl 3.1, MgCl_2 4, CaCl_2 5, sucrose 50, HEPES 10, pH 7.4 adjusted with NaOH) using a gravity perfusion system positioned within 50 μm from the cell body and patch pipettes (borosilicate glass capillary tubes: GC 150T-10; Clark Electromedical Instruments, Harvard Apparatus). The latter were filled with internal solution containing (in mM): K-D-gluconic acid, 160; NaCl, 10 mM; MgCl_2 , 1 mM; CaCl_2 , 0.5; K-fluoride, 10; ATP Mg, 3; EGTA 10; HEPES, 20 and pH adjusted to 7.4 with KOH. Pipettes had resistances ranging from 0.9 to 1 M Ω when filled with internal solutions. Repeated successive applications of 10 μM neonicotinoid solutions were carried out by pneumatic pressure ejection (15 psig, Miniframe, Medical System Corporation, USA). The pressure ejection was made through a glass micropipette, resistance 1.8 M Ω , positioned in solution within 100 μm from the isolated cell body. The dose–response curve was derived from the fitted curve using the same equation as described above, in which Y is the normalised response, I_{\max} and I_{\min} are the maximum and minimum responses, H is the Hill coefficient, EC_{50} is the concentration giving half the maximum response and X is the logarithm of the compound concentration. All compounds tested were purchased from Sigma Chemical Company (France).

3. Results and discussion

3.1. X-ray diffraction and crystal structures analyses

In this section, we start by describing the crystal structures resolved in the present work and compare them to the data available in the literature. An assessment of the molecular interaction potential of the three neonicotinoids is then performed at the light of these new data and of the knowledge on the interaction of neonicotinoids with nAChRs.

3.1.1. Molecular structures

3.1.1.1. Dinotefuran. The atom numbering of DIN is indicated on Figure 1 whereas Figure 2 provides the corresponding ORTEP representation. The C5–C4–C3–N3 and C4–C3–N3–C2 torsional angles, governing the relative orientation between the TFM and the guanidine moieties, have respective values of -179° and 83° . The furanyl ring presents an envelop conformation with the C7 methylene carbon out of the plane (C4–C5–C6–O3 = -8° and C5–C6–O3–C7 = -16° , respectively). The conjugated nitro guanidine group and the furanyl ring belong to two parallel planes, the O3 oxygen atom being at the opposite side of the nitro group.

The structural features of the nitroguanidino (DIN, IMI) or cyanoimino (ACE) pharmacophore moiety of the neonicotinoids investigated in the present work are key elements for their interactions with nAChRs.^{6,50} The C2–N2 double bond of DIN has the classical *E* configuration of neonicotinoids. The nitroguanidine moiety is planar and characterised by distances indicating a strong conjugation between the donor N3 and N1 groups and the acceptor nitro function. The C2–N1 and C2–N3 bonds are significantly shorter (1.32 and 1.34 Å) than the C3–N3 and C1–N1 bonds, (1.46 and 1.44 Å) which is consistent with the double bond nature of the former. In the same vein, the C2–N2 double bond, of 1.36 Å, is slightly longer than a typical imine double bond (1.33 Å).⁵¹ Lastly, the N2–N4 bond is shorter (1.34 Å) than a typical N–N bond (H₂N–NO₂: 1.43 Å)⁵¹ also hinting to a double bond character. These features indicate the electronic delocalisation of the N1 and N3 lone pairs to the nitro substituent. Indeed, the nitro electron-withdrawing tip of DIN is coplanar with the guanidine moiety, allowing the electronic flow characteristic of neonicotinoids (N1–C2–N2–N4 and N3–C2–N2–N4 of 178 and -1°).^{50,52,53} In the guanidine fragment, the two NH groups are in *anti* position with respect to each other and the nitro substituent is oriented to yield an intramolecular N1H...O1 interaction ($d(\text{H}\cdots\text{O1}) = 1.82 \text{ Å}$).

3.1.1.2. Imidacloprid. Table 1 compares selected geometric parameters of the IMI crystal structures resolved in the present study to those available in the literature. The numbering convention of IMI is indicated on Figure 1 and Figure 3 shows the ORTEP representations of the two independent molecules (1 and 2 in Table 1) of the asymmetric unit cell. The C9–C5–C4–N3 and C5–C4–N3–C1 dihedral angles, governing the orientation between the two rings, have respective values of $+18^\circ$; -92° and $+156^\circ$; $+89^\circ$ in these two molecules. These conformations significantly differ from previously identified structures in the CSD (HANFOS, corresponding dihedral angles of 63° ; -107°)⁵⁴ or in Kagabu and co-worker's investigation (torsional angles of -63° et $+107^\circ$).⁵⁰ The two latter were in fact symmetry related with respect to the prochiral methylene C4. The C9–C5–C4–N3 torsional angle of 1 is close to the one observed in the binding site of AChBP

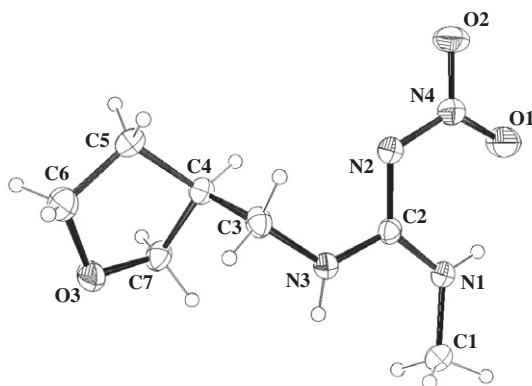


Figure 2. ORTEP representations (DIN).

Table 1

Selected geometric parameters (angles ($^\circ$)) of IMI in the solid state

Name/ refcode	C9–C5– C4–N3	C5–C4– N3–C1	N3–C3– C2–N1	C3–C2– N1–C1
1 ^a	+18	−92	+2	0
2 ^a	+156	+89	−14	+13
HANFOS ⁴¹	+63	−107	+7	−5
3 ³⁸	−63	+107	−6	+4
3C79 ¹¹	+24	+83	+1	0

^a This work.

(respective dihedral angles of $+17^\circ$ and $+24^\circ$). This is not the case for the C5–C4–N3–C1 dihedral angle, the nearly opposite values measured in 1 and the AChBP-bound structure (-92° and $+83^\circ$, respectively) leading to opposite orientations of the imidazolidine ring and the attached nitroimine fragment in the two structures. In all crystal structures the imidazolidine ring conserves its planarity, the N3–C3–C2–N1 and C3–C2–N1–C1 ranging from -14° to $+7^\circ$ and from -5° to $+13^\circ$, respectively. Figure 4 shows two views of the superposition, on the CPM fragment, of the five crystal structures. This Figure clearly illustrates the flexibility around the methylene inter-ring bridge and the consequences in terms of conformational space swept by the five-membered imidazolidine ring. As well as observed in DIN crystal structure, the nitroguanidine moiety is strongly conjugated in IMI. Indeed, the $d(\text{N3C1})$ values, of 1.34 Å, are significantly shorter than the $d(\text{N3C4})$ distances (of 1.45 Å), the $d(\text{C1N2})$ have values from 1.34 to 1.35 Å and the $d(\text{N2–N4})$ distances of 1.35 Å, are significantly smaller than the typical N–N bond (H₂N–NO₂: 1.43 Å).⁵¹ Another noticeable structural feature is that both molecules are characterised by intramolecular N1H...O1 HB that reach 1.99 and 2.05 Å. These values are in the line of those reported by Chopra (2.03 Å)⁵⁴ and by Kagabu (2.02 Å),⁵⁰ but significantly longer than that observed in DIN X-ray structure. We attribute this decreasing to the geometry of the cyclic nitroguanidine moiety, characterised in particular by a value of the N1–C1–N2 valence angle inferior to the ideal value of 120° , forcing a deviation from the ideal planar intramolecular HB.⁵⁵

3.1.2. Molecular packing/Hydrogen-bonding interactions

A crystal structure is an archetypal supermolecule that provides direct experimental evidence on the intermolecular interactions controlling molecular aggregation. In the case of small biological ligands, this information can be used in rational drug design.⁵⁶

3.1.2.1. Dinotefuran. The HB geometric parameters that have been measured in the crystal structure of DIN are listed in Table 2. In the solid state, the DIN molecules are associated as hydrogen-bonded dimers, the furanyl oxygen atoms and the NH groups respectively behaving as HB acceptors and donors (Fig. 5). The measured N3H...O3 distance is of 2.024 Å. These HB are roughly parallel to the *b* crystallographic axis. The oxygen atoms of the nitro group are also involved in HB, O1 with an H atom of the C1 methyl group (2.511 Å) and with N1H (2.559 Å), N1H being implied in a three-centre HB, O2 with the C5 methylene group of the furanyl ring (2.558 Å). On the basis of the HB distances, these interactions appear weaker than the previous N3H...O3 but remain significantly shorter than the sum of H and O van der Waals radii (2.62 Å), the classical criterion to determine the existence of HB in the solid state.⁵⁷ In view of the established role of the nitro group in the binding to nAChRs,^{15,19,57} these interactions are probably nonnegligible.

3.1.2.2. Imidacloprid. Table 2 presents the HB parameters (distances, angles) measured in the present work and reported in the literature for IMI and Figure 6 shows the HB involved in the crystal

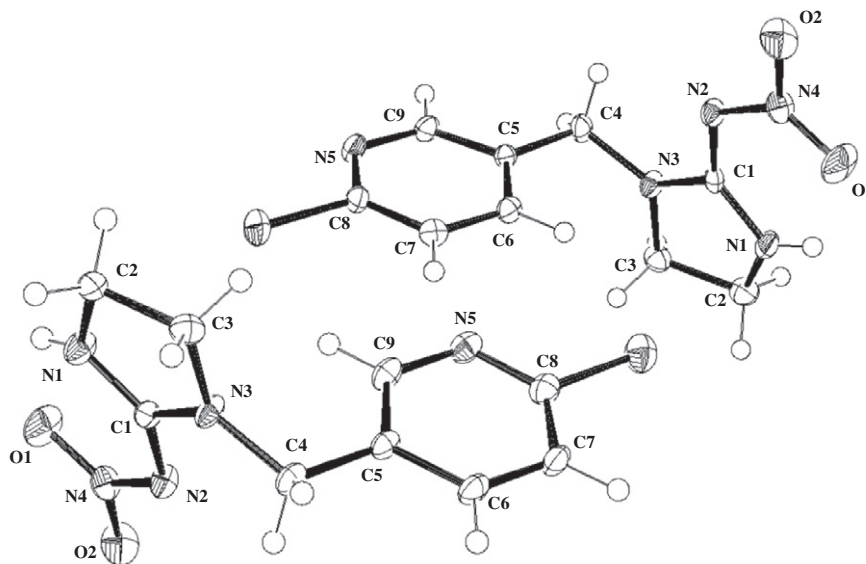


Figure 3. ORTEP representations (IMI).

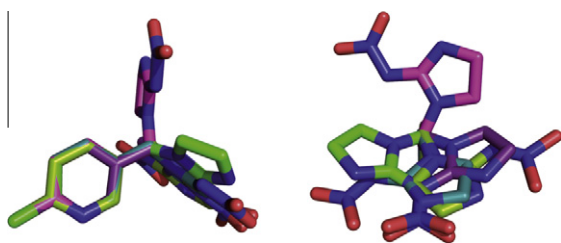


Figure 4. Overlay of the five crystal structures of IMI viewed according to different perspectives showing the various possible orientations of the imidazolidine and nitroimine fragments.

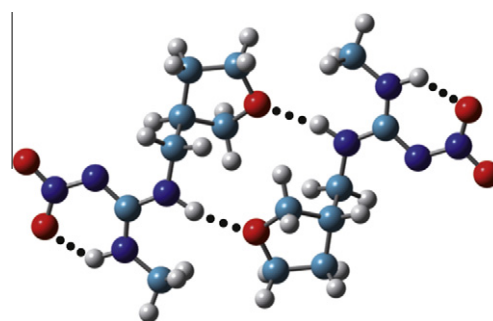


Figure 5. HB interactions in the crystal structure of DIN.

Table 2

Geometric parameters (distances (Å), angles (°)) of HB observed in the crystal structures of DIN, IMI and ACE

Name/CSD refcode	D-H...A	<i>d</i> (H...A)	<i>θ</i> (D-H...A)	<i>φ</i> (H...AY)
DIN ^b	N1-H...O1 ^a	1.817	129	106
	N3-H...O3	2.024	163	141
	C5-H...O1	2.563	141	104
	N1-H...O2	2.559	124	105
	C1-H...O2	2.515	126	154
IMI (1, 2) ^b	N1a-H...O1a ^a	1.987	115	110
	N1a-H...N5b	2.114	144	121
	C2a-H...O2b	2.400	123	139
	C3a-H...O2b	2.402	124	162
	C6a-H...O1b	2.309	130	153
	N1b-H...O1a	2.125	128	118
	C7b-H...N5a	2.281	164	120
IMI (HANFOS) ⁴¹	N1-H...O1 ^a	2.022	112	111
	N1-H...O1	2.061	139	127
	C3-H...O2	2.329	120	157
IMI (3) ³⁸	N1-H...O1	2.029	112	111
	N1-H...O1	2.049	143	129
	C3-H...O2	2.390	116	157
ACE (HANBAA)	C7-H...N3	2.313	158	136

For imidacloprid, the labels *a* and *b* refer to the two independent molecules of the asymmetric unit.

^a Intramolecular HB.

^b Crystal structures resolved in the present study.

packing of the IMI structure obtained in the present work. Interestingly, the molecular packing and HB interactions observed in the

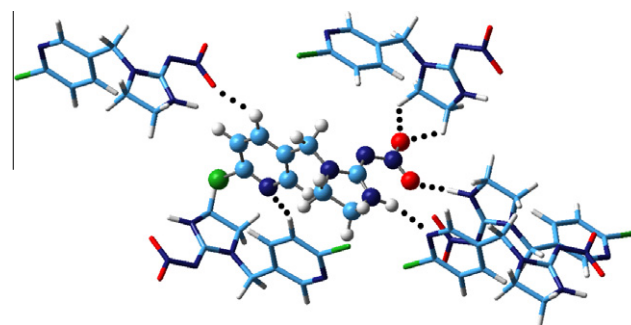


Figure 6. HB interactions in the crystal structure of IMI obtained in the present work.

structure crystallised herein are different from the previously reported data for this neonicotinoid. The asymmetric unit of the crystal is formed of two independent molecules with two different conformations, and involved in different HB networks. Thus, in contrast to the previous IMI crystal structures, the pyridinic nitrogen N5 of the two molecules uses its HB potential, with H...N5 distances of 2.11 and 2.28 Å and XH...N5 valence angles of 144 and 164° for N1aH...N5b and C7b-H...N5a, respectively. The other HB are more similar to previously-reported data for IMI crystals (Table 2);^{50,54} this is the case, on the one hand, for the N1b-H...O1a interaction, with a *d*(H...O1) of 2.13 Å and N1H...O1 angle of 128°

and, on the other hand, for both C2aH...O2b and C3aH...O2b having almost the same features as the one reported by Chopra⁵⁴ and Kagabu.⁵⁰ These latter interactions, involving CH HB donors, are longer than the previous ones but shorter than the sum of the van der Waals radii of the atoms involved (2.62 and 2.65 Å for H...O and H...N interactions). Eventually, an HB involving another CH donor of the pyridinic ring (C6H) participates in the crystal arrangement: it corresponds to the C6aH...O1b interaction, with respective d(H...O1) distance and C6H...O1 angle of 2.31 Å and 130°. This interaction is observed for the first time. The Cl...Cl short contacts discussed in HANFOS⁵⁴ are not observed in this structure.

3.1.2.3. Acetamiprid. One crystal structure of ACE (Fig. 1) is found in the CSD under the HANBAA refcode.⁵⁸ No conventional HB donors are available in the chemical structure of ACE and only CH donors can possibly be involved in HB. Indeed, in the solid state, the nitrogen atom N3 of the tip nitrile group is engaged in a HB with a CH group (C7H) of the pyridine ring ($d(\text{C7H}\cdots\text{N3}) = 2.313$ Å, $\text{C7H}\cdots\text{N3} = 158^\circ$). The HB donor capacity of the C7H group is enhanced compared to an unsubstituted pyridinic CH due to the electron-withdrawing character of the chlorine substituent. The chains formed through these interactions extend along the *c* crystallographic axis. Another interesting feature of this crystal structure is the existence of π stacking interactions between the amidine group and the pyridine ring, the distance between the centroid of the six-membered ring and the imino nitrogen of the amidine substituent being of 3.48 Å. Such interactions are worth mentioning owing to the pointing out of co-operative π - π and HB interactions in the binding of neonicotinoids to nAChRs.⁵

3.1.3. Comparison with interactions in AChBP environments

Among the three neonicotinoids, only IMI has been co-crystallized with AChBP,^{15–17} the structural and functional surrogate of nAChRs. With *Lymnea stagnalis* AChBP, the surrogate of vertebrate nAChRs, the nitrogen atom of the pyridine ring forms a HB with the amide group of Met114 and the carbonyl group of Leu102 in loop E via a water molecule,¹⁷ as observed in the AChBP binding sites of nicotine⁵⁹ and epibatidine.⁶⁰ The guanidine moiety of IMI is found to stack with the aromatic ring of Tyr185.¹⁷ Lastly, the nitro group of IMI appears implied in HB interactions with the amide group of Gln55.¹⁷ With *Aplysia californica* AChBP, the surrogate of insect nAChR, the interactions are very similar both in the vicinity of the pyridine ring and the guanidine fragment, which stacks with the aromatic ring of Tyr188.¹⁶ Nevertheless, a noticeable difference concerns the interactions established with the nitro group, several HB donor groups of AChBP residues being in close contact with the nitro oxygen atoms: OH groups of Tyr 55 and Ser189, NH peptidic group of Cys190 and NH₂ of the Gln57 amide.¹⁶

In a recent molecular modelling investigation, similar interactions have been predicted for DIN: the oxygen atom of the tetrahydrofuran ring is part of a water mediated HB with both Leu102 and Met114 whereas the nitroguanidine moiety is involved in a stacking interaction with Tyr188 and the nitro tip oxygen undergoes hydrogen bonding with the Cys-190 backbone NH.¹⁹ To our knowledge, such data are not available for ACE. Nevertheless, the structural information available in AChBP environments is not sufficient to reach an atomic-scale understanding of the structural and HB properties of the three neonicotinoids. Subsequently, a comparison of the trends observed in small crystals may provide useful data.

It is worth noting that the electronic conjugation and planarity characteristic of the $[-\text{N}-\text{C}(\text{E})=\text{X}-\text{Y}]$ moiety of the neonicotinoid pharmacophore should have significant consequences on the HB features of the tip functional group (nitro or nitrile according to

the neonicotinoid). In the case of nitriles and carbonyles, we have shown that such electronic effects lead to a significant increase of HB strength.^{61–64} While the nitro group is generally viewed as a poor HB acceptor, let us highlight that the HB lengths involving NH donors in IMI structures (range of 2.02 to 2.13 Å) are indeed significantly shorter than the overall $d(\text{H}\cdots\text{O})$ bond length of 2.30(1) Å reported by Allen et al. from a statistical analysis of (N/O)H...O-nitro HB (620 HB) observed in the CSD.⁶⁵ In the same vein, the $d(\text{H}\cdots\text{O})$ bond length involving CH donors are ranging from 2.31 to 2.40 Å and are shorter than the Steiner's reference CH...O contacts for nitro groups (from 2.48(4) to 2.63(3) Å depending on the nature of the CH group).⁶⁶ Lastly, it appears that the HB observed for nitroimine derivatives show a directional preference for the oxygen nitro lone pairs, the average HON angle being of 136°, quite close to the ideal 120° typical of an oxygen atom in such environment. When only NH donor groups are taken into account, the corresponding average value is of 119°. These trends indicate a stronger interaction than in conventional nonconjugated nitro groups that lack of clear-cut directional preference.⁶⁷ In the case of ACE, the analysis should be performed more carefully since no systematic investigation devoted to CH...N \equiv C interactions that could be used as a landmark is found in the literature. However, even if it appears longer than those found in (N/O)H...N \equiv C HB (from 1.99 to 2.09 Å),⁶³ this CH...N \equiv C interaction $d(\text{H}\cdots\text{N3}) = 2.313$ Å is significantly shorter than the sum of van der Waals radii limit of involved atoms (2.65 Å).

The results obtained in the present study show that DIN possesses the structural features of neonicotinoids, and specifically it presents a planar 'push-pull' nitroimine moiety. The crystal structures reported for IMI bring new light in terms of conformation and HB interactions, since the structures adopted and some of the HB observed are different from previously reported data. Lastly, a relation between the electronic flow characteristic of the pharmacophore of neonicotinoids and the HB accepting power of the tip nitro group is pointed out in the case of IMI. We have focused in the present work on the examination of the relative structural and HB interactions features of the three neonicotinoids. Since π - π interactions have been shown to occur co-operatively in the binding process, an investigation devoted to the deciphering of their contribution would be interesting. However, such contributions, more difficult to evaluate owing to their dispersive and nonspecific character, must be founded on a study taking into account the receptor environment, an objective which is beyond the scope of the present work.

3.2. Quantum chemistry calculations

In this part of the manuscript, the conformational features of the three neonicotinoids obtained through DFT calculations are presented and analysed in conjunction to the experimental data available. A qualitative discussion on their respective HB properties

Table 3

Gibbs energy differences and relative populations of the twelve more stable dinotefuran conformers calculated at the LMP2/aug-cc-pVTZ(-f)//MPWB1K/6-31+G(d,p) level

	DIN-1-N1	DIN-2-N1	DIN-3-N1	DIN-4-N1
$\Delta G/\text{kJ mol}^{-1}$	0.0	1.6	6.2	6.7
p_i	46.6%	24.1%	3.7%	3.1%
	DIN-5-N1	DIN-6-N1	DIN-7-N1	DIN-8-N1
$\Delta G/\text{kJ mol}^{-1}$	9.0	9.1	9.3	9.5
p_i	1.2%	1.2%	1.1%	1.0%
	DIN-1-N3	DIN-2-N3	DIN-3-N3	DIN-4-N3
$\Delta G/\text{kJ mol}^{-1}$	3.8	6.5	7.1	8.1
p_i	10.2%	3.3%	2.6%	1.8%

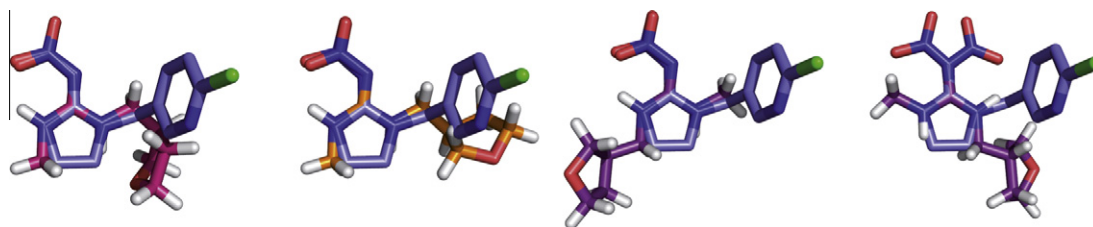


Figure 7. Overlays of the IMI AChBP bound structure (blue) with DIN-1-N1 (pink), DIN-2-N1 (orange) and DIN-1-N3 (yellow).



Figure 8. Structures of the three main DIN conformers.

from theoretical descriptors based on molecular electrostatic potential calculations is also presented.

3.2.1. Conformational analysis-pharmacophore orientations

DIN is characterised by several degrees of freedom such as the relative orientation between the furanyl and guanidine moieties, the conformation of the furanyl ring and the rotations around the N3–C2 and N1–C2 bonds. Thirty stable conformational isomers have been identified, twelve of them having at least a relative population of 1% (see Table 3). These conformations can be divided into two sets differentiated by a chelation occurring between the N1H or N3H and the nitro groups. The former set (named DIN-*i*-N1 in Table 3 and representing 82% of the whole population)

gathers conformers which could roughly match the IMI AChBP bound structure whereas the latter set (DIN-*i*-N3) includes significantly different conformers (Fig. 7). This discrepancy might be important in regards of the interaction of DIN with the residues of the nAChR binding site. Three conformations (Fig. 8) seem significantly preponderant in comparison to the others. In the absolute minima, two intramolecular HB, involving both N1H and the N3H groups occur. The furanyl ring of this strongly chelated form does not overlay the pyridinic ring of the IMI AChBP bound structure, but it could favour its lipophilic character, a physicochemical property important for an optimum activity of neonicotinoids, for example during root uptake in seed treatment applications. Indeed, these intramolecular interactions should increase the lipophilicity of the structure thanks to a decrease of the HB basicity of its acceptor sites. The second minimum DIN-2-N1, +1.6 kJ mol^{−1} above DIN-1-N1, corresponds to the conformation found in the crystal-line structure of DIN obtained in the present work.

To our knowledge, only one previous conformational investigation of IMI has been achieved, but was carried out using the semi-empirical approach.⁶⁸ The different degrees of freedom investigated in the present study are the rotations around the C5–C4 and C4–N3 bonds linking the two rings and the conformation of the imidazolidine ring. We located eight different conformers of IMI, distinguishable by the rotations around the methylene

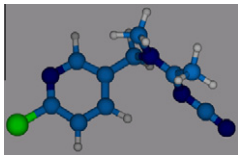
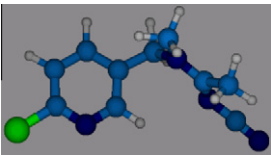
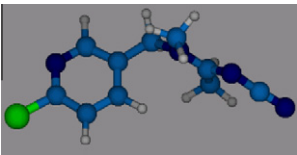
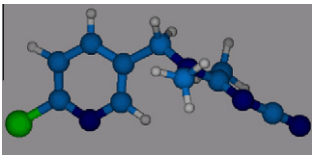
Table 4

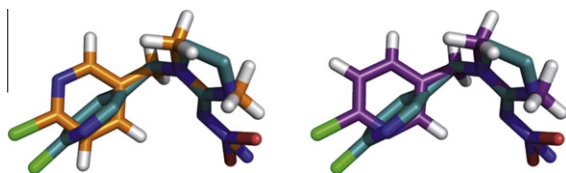
Structures, Gibbs energy differences and relative populations of IMI conformers calculated at the MPWB1K/6-31+G(d,p) level

		ΔG /kJ mol ^{−1}	p_i			ΔG /kJ mol ^{−1}	p_i
IMI-1a (3C79)		0.0	26.3%	IMI-1b		0.0	26.3%
IMI-2a		1.3	15.3%	IMI-2b		1.3	15.3%
IMI-3a		4.4	4.5%	IMI-3b		4.4	4.5%
IMI-4a		4.7	3.9%	IMI-4b (HANFOS)		4.7	3.9%

Table 5

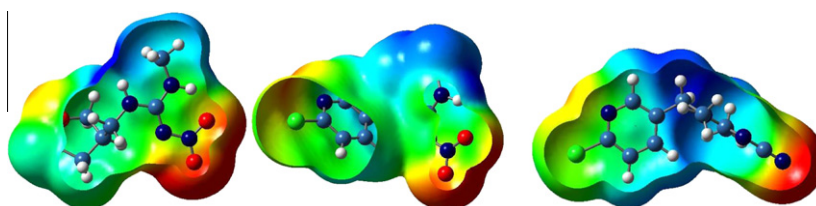
Structures, Gibbs energy differences and relative populations of ACE conformers calculated at the MPWB1K/6-31+G(d,p) level

	ACE-1	ACE-2	ACE-3	ACE-4
				
$\Delta G/\text{kJ mol}^{-1}$	0.0	6.0	7.9	8.5
p_i	86.1%	7.6%	3.6%	2.8%

**Figure 9.** Overlays of the AChBP bound IMI crystal structure (blue) with selected energetic minima of ACE (ACE-1 (orange) and ACE-2 (yellow)).**Table 6**Weighted minimum electrostatic potential values V_{\min} (kJ mol^{-1}) calculated for IMI, ACE and DIN

V_{\min}	$\text{NO}_2\text{-O}_{\text{free}}$	$\text{NO}_2\text{-O}_{\text{linked}}$	N_{pyr}	N_2
IMI	−219.8	−212.4	−205.0	−158.6
V_{\min}	$\text{N}\equiv\text{C}$		N_{pyr}	$\text{N-C}\equiv\text{N}$
ACE	−256.9		−203.7	−126.9
V_{\min}	$\text{NO}_2\text{-O}_{\text{free}}$	$\text{NO}_2\text{-O}_{\text{linked}}$	O_{fur}	N_2
DIN	−253.5	−244.8	−159.2 (−182.8)	−225.7

group and a slight distortion of the imidazolidine ring. As already observed from the analyses of the crystal structures, the prochiral methylene carbon atom C4 induces the co-existence of pseudo-enantiomers presenting exactly the same energetic values and physicochemical properties (ranked by line in Table 4). In fact, our results indicate a very flexible IMI, the energetic minima covering a range of 5 kJ/mol. Therefore, the HANFOS crystal structure found in the CSD is located about 5 kJ mol^{-1} above the absolute (isolated) minimum, whereas the AChBP bound IMI structure does not correspond to an energetic minimum on the DFT potential energy surface. One of the independent molecule of the asymmetric unit of the crystal structure reported in this work is close to AChBP bound IMI structure considering the quasi symmetry equivalence of the structures generated by rotation of 180° around the C5–C4–N3–C1 torsion angle (respective values of -92 and $+82^\circ$). However, if these conformers have identical properties, the asymmetric environment of the biological receptor will induce different interactions. The structural features of the second independent molecule of our crystal structure do not correspond to an energetic minimum on the theoretical potential energy surface.

**Figure 10.** Molecular electrostatic potential surfaces of selected IMI, ACE and DIN conformers.

Four out of the eight conformers identified for ACE present a significant proportion and the global minimum, ACE-1, accounts for more than 86% of the total population (Table 5). Moreover, it corresponds to the experimental crystalline structure (HANBAA refcode in the CSD). The four main minima differ by the relative orientations of the chloropyridine ring and the methyl groups (Table 5). None of these conformers perfectly match the AChBP-bound IMI solid-state structure,¹⁶ with consideration of their two potential interaction sites, that is the pyridine nitrogen and either the nitro or the cyano group. Nevertheless, a rather satisfying overlay is obtained between IMI and ACE-2, their lone pair roughly pointing towards the same direction, despite a significant rotation of the pyridinic nitrogen between the two structures (Fig. 9). Moreover, the energy barrier (16 kJ/mol in ΔG scale) between ACE-1 and ACE-2 is low enough to be easily overcomable at physiological temperature.

3.2.2. HB properties of DIN, IMI and ACE

3.2.2.1. HB Donor properties. Besides HB acceptor sites, DIN and IMI contain NH groups that can potentially act as HB donors with residues of the receptor binding site. On the contrary, ACE can only act as an HBA. The only NH group present in IMI is involved in the intramolecular interaction with the nitro group and thus shows a quite weak $V_{\alpha}(r)$ value ($+823.2 \text{ kJ mol}^{-1}$). The chelation is probably significantly stronger in DIN since the $V_{\alpha}(r)$ value of the corresponding chelated NH group is even weaker ($+750 \text{ kJ mol}^{-1}$) in agreement with the experimental and theoretical shorter $\text{NH}\cdots\text{O}$ distance. This is confirmed by an AIM analysis around this $\text{NH}\cdots\text{O}$ interaction that unravels a bond critical point with an electron density, ρ_{BCP} , of 0.0398 in DIN, significantly above IMI ρ_{BCP} (0.0295). However, there is an additional NH group in DIN that may act as an HBD for the binding site residues and it exhibits a much more sizable $V_{\alpha}(r)$ value ($+905 \text{ kJ mol}^{-1}$) when the chelated $\text{NH}\cdots\text{O}$ conformers are not considered, such as in DIN-1-N1. Accordingly, DIN is a significantly stronger HBD than *N*-methylacetamide, the conventional model of the peptidic bond characterised by $V_{\alpha}(r) = +840 \text{ kJ mol}^{-1}$.

3.2.2.2. HB Acceptor properties. The minimum electrostatic potential V_{\min} has been computed in the vicinity of each heteroatom (Table 6) and molecular electrostatic potential maps of neonicotinoids have been determined (Fig. 10). From these theoretical data, qualitative tendencies of the relative HB accepting strengths of the

three neonicotinoids can be deduced. The cyano moiety of ACE appears as a significantly stronger HB acceptor than the nitro group of IMI, but the latter may be involved in additional interactions.

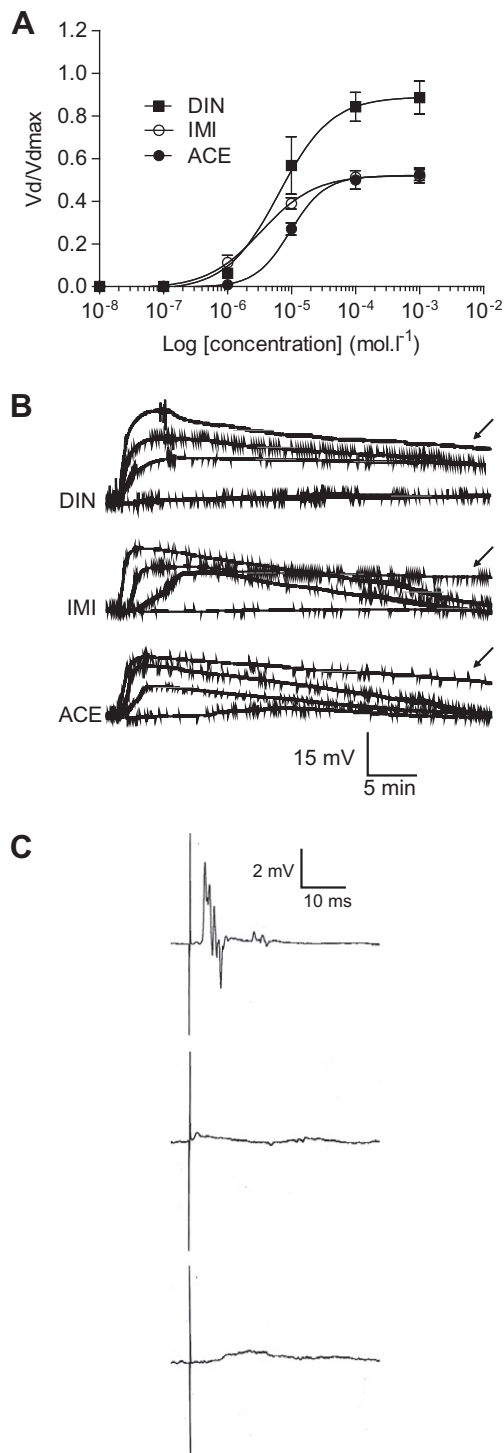


Figure 11. Effect of DIN, IMI and ACE on synaptic nAChRs. (A) Semi-logarithmic dose–response curves of IMI, ACE and DIN. Data are pooled from 6 preparations and mean values of the amplitude of peak depolarisation are plotted. Error bars represent mean \pm M.E.N. (B) Neonicotinoids induced depolarisations after bath application of 1 μM , 10 μM , 100 μM and 1 mM. Arrows indicate that at higher concentrations, we did not observe a recovery. (C) Typical examples showing the blocking of the compound excitatory postsynaptic potential at 1 mM neonicotinoids. Upper trace: before neonicotinoid applications, middle trace: when the ganglionic depolarisation reached a peak, lower trace: 40 min after bath application of neonicotinoids.

Keeping this ‘multi-interaction’ ability, the nitro moiety of DIN is found to be as strong as the ACE cyano group. Table 6 shows that the oxygen atoms of DIN’s nitro group display significantly weaker V_{min} values (from about 35 kJ/mol) than in IMI’s nitro group. We explain this difference by the influence of the electron-withdrawing effect of the chloropyridinyl substituent, an analysis substantiated by the similar V_{min} values obtained when the 6-chloropyridine and furanyl fragments of IMI and DIN are removed (–240.0 and –248.0 kJ/mol, respectively). The remaining 8 kJ/mol difference is rationalised by the influence of the intramolecular HB interaction $\text{N1H}\cdots\text{O1}$, significantly stronger in DIN ($d(\text{H}\cdots\text{O1}) = 1.800 \text{ \AA}$) than in IMI ($d(\text{H}\cdots\text{O1}) = 1.938 \text{ \AA}$), which parallels the crystallographic observations (Table 2). The calculation of V_{min} of nitromethane (–173.4 kJ/mol), an aliphatic derivative, confirms the influence of an extensive electron delocalization in the V_{min} increase in DIN (–253.5 kJ/mol) and IMI (–219.8 kJ/mol) and the expected increase of HB strength of the nitro group of DIN and IMI. The same effects apply on the cyano group of ACE ($V_{min} = -221.8$ and –256.9 kJ/mol for acetonitrile and ACE, respectively) although weakened by the electron-withdrawing character of the chloropyridinyl substituent, as in IMI. *N,N*-dimethylcyanoacetamide, the fragment without this chloropyridine substituent, indeed shows a V_{min} value of –275.0 kJ/mol. For nitriles, we have shown that such variation leads to an enhancement of HB strength of 7.6 kJ/mol.⁶³

The pyridinic nitrogen atoms have roughly the same HB basicity ability and are significantly stronger HBAs than the furanyl oxygen of DIN. It is worth noticing that the HB basicity of the oxygen atom of the furanyl is weak owing to its possible involvement in an intramolecular $\text{NH}\cdots\text{O}$ interaction, and that the weighted V_{min} value increases to –182.8 kJ mol^{–1} if only conformers free of this

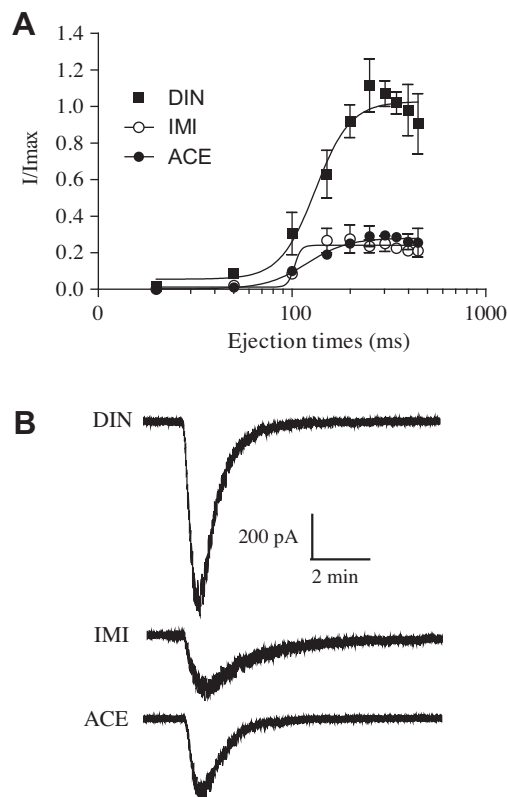


Figure 12. DIN, IMI and ACE-induced currents on DUM neurons. (A) DUM neuron responses to consecutive applications of 10 μM neonicotinoids at a holding membrane potential of –50 mV. Repeated applications of neonicotinoids were made with 2 min interval duration between the end of one application and the beginning of the next. Each current was normalised to the maximum current amplitude obtained at 300 ms DIN. (B) Typical example of DIN, IMI and ACE-induced currents obtained in the same conditions at 300 ms pulse duration.

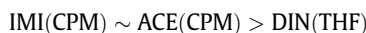
second chelation are considered. Finally, the nitrogen atoms N2, which bear the nitro or cyano group, also appear as significant HB acceptor sites, the strongest being found in DIN. It is therefore surprising that this potential HB site remains unseen in the available crystal structures. This observation probably originates in steric hindrance, the imino nitrogen being approximately located in the middle of the conjugated chain.

3.2.3. Relevance for DIN, IMI and ACE binding site interactions

In the absence of AChBP–neonicotinoid structural data of sufficient precision, physico-chemical studies devoted to the characterisation of neonicotinoid properties are very useful to reach a comprehensive understanding of their biological activity. On the one hand, a stronger HBA ability is found with neonicotinoids bearing a pyridinic nitrogen rather than with a furanyl oxygen. On the other hand, both ACE and DIN appear having a stronger HBA site than IMI with their cyano and nitro moieties, respectively. However, the nitro group is a polybasic site (contrary to the cyano moiety) and this property can be fulfilled in the receptor environment, where several HB donor groups can be available. Finally, the molecular electrostatic potential calculations point out the HB ability of the imino nitrogen of DIN, which has a significantly more negative V_{\min} compared to corresponding values in IMI and ACE. With respect to the ‘push–pull’ moiety of the neonicotinoid pharmacophore, the order of HB accepting strength suggested for the three neonicotinoids is:



With respect to the other fragment (CPM or THF) of these compounds, the following order of HB accepting strength is obtained:



3.3. Agonist actions of DIN, IMI and ACE at synaptic and extrasynaptic nicotinic receptors

Neonicotinoid insecticides are of biological interest because they are originally related insecticidal compounds with a structural similarity to nicotine and a common mode of action. Thus, they have been shown to act as full and partial agonists of extrasynaptic *nAChRs*.⁶⁹ Indeed, using isolated cell bodies, it has been demonstrated that ACE is a full agonist while IMI is a partial agonist.^{70,71} However, to the best of our knowledge, no direct comparison of the three neonicotinoid actions on both synaptic and extrasynaptic *nAChRs* is found in the literature. Here, electrophysiological analyses are performed and compared at cockroach synaptic and extrasynaptic *nAChRs* from the sixth abdominal ganglion. First, using the mannitol-gap method, a significant difference of biological effect between the three neonicotinoids is observed. Thus, DIN appears more effective on synaptic *nAChRs* than IMI and ACE and demonstrates a strong dose-dependent increase of the ganglionic depolarisation (Fig. 11A and B). Nevertheless, in all data, our results show that DIN, IMI and ACE are able to block the amplitude of compound excitatory postsynaptic potentials when the neonicotinoid-induced depolarisation reached a peak, confirming that they act at postsynaptic *nAChRs*^{49,46,72} (Fig. 11C). Indeed, preliminary experiments performed at synapses between cockroach cercal afferent nerve XI and the giant interneurons demonstrated that bath application of IMI induced a dose-dependent depolarisation of postsynaptic *nAChRs* in which the compound excitatory postsynaptic potentials are blocked.⁴⁶ We demonstrate also that neonicotinoids are able to produce desensitization of postsynaptic *nAChRs* at higher concentrations which is not reversible after wash-out. Interestingly, when the agonist effects of DIN, IMI and ACE on synaptic *nAChRs* are compared to those obtained on extrasynaptic *nAChRs*,

the greater efficiency of DIN compared with IMI and ACE (Fig. 12A) is corroborated. It is worth noticing that in our method, we used 10 μM successive applications of DIN, IMI and ACE solutions and that the neonicotinoid doses are elevated by progressively raising the length of the pressure ejection pulse, using the same cell.^{49,73} In these conditions, the maximal DIN-induced current is -1.02 ± 0.06 nA (at 300 ms and -50 mV holding potential) while it is -0.26 ± 0.08 nA and 0.28 ± 0.01 nA for IMI and ACE, respectively (Fig. 12B). These data are consistent with previous studies demonstrating that DIN is a full agonist inducing more than 80% of the ACh-induced currents while IMI is a partial agonist.^{70,71} Interestingly, we found that ACE is not able to induce a strong ionic current at this lower concentration (10 μM and 300 ms pulse duration) demonstrating that it is a weak agonist of cockroach DUM neuron *nAChRs* compared to DIN. Indeed, a high agonist binding site for DIN has been previously identified using cockroach nerve cord.⁷⁴ In our study, we found also that in addition to its agonist effect on DUM neuron *nAChRs*, DIN-induced current amplitudes decrease from -1.02 ± 0.06 nA at 300 ms to -0.86 ± 0.16 nA at 450 ms (Fig. 12A) suggesting a possible *nAChRs* saturation (or desensitization). The present electrophysiological data support the finding that DIN, IMI and ACE differently act as agonists of both synaptic and extrasynaptic *nAChRs*. Indeed, it has been demonstrated that neonicotinoid effects involved two distinct nicotinic receptor subtypes. In *Nilaparvata lugens*, imidacloprid has two distinct binding sites⁴ which are attributable to the existence of different *nAChR* subtypes. Thus, co-immunoprecipitation studies reveals that *nAChR* subtypes containing $\text{N}\alpha 3$, $\text{N}\alpha 8$ and $\text{N}\beta 1$ subunits constitute the higher affinity binding site whereas *nAChR* subtypes with $\text{N}\alpha 1$, $\text{N}\alpha 2$ and $\text{N}\beta 1$ subunits contain the lower affinity binding site.⁷⁵ This pharmacological effect could be associated to specific mutations in the $\text{N}\alpha 1$ subunit such as Y151S.⁷⁶ At all events, further studies are required to investigate the possible correlations between the electrophysiological and chemical properties.

4. Conclusions

New experimental, theoretical and electrophysiological data on DIN, IMI and ACE, some of the most widely used neonicotinoids, have been obtained. The X-ray structure of DIN shows a planar arrangement of the electronegative pharmacophore, a feature characteristic of this class of insecticides allowing an electronic communication from the push amino to the pull nitro groups. Several HB interactions participate in the crystal arrangement, involving the functional groups (nitro, furanyl oxygen) identified in the binding to *Aplysia* AChBP. Interestingly, the conformations and HB interactions observed in the new crystal structures of IMI differ from previously reported features. The analyses of the HB geometries observed in the IMI crystal structures available indicated an enhanced HB strength of the nitro group due to extensive electron delocalization. The DFT calculations allowed the identification of the main energetic minima of the three neonicotinoids. These compounds are highly flexible, the key conformers being located in a narrow energetic range of about 10 kJ/mol for DIN and ACE and 5 kJ/mol for IMI. This flexible character is reflected in the different conformations observed in small crystal structures and AChBP environments. Molecular electrostatic potential calculations provided a qualitative HB ranking of the molecular fragments constituting the three neonicotinoids. DIN possesses the electronegative fragment with the strongest HB acceptor (nitro group), the cyano group of ACE being a close second. In the same vein, the pyridinic nitrogen of CPM neonicotinoids (IMI and ACE) is a significantly better HB acceptor than the furanyl oxygen of DIN. In short, the present study brings new light on the chemical

features (structural and interactions) of DIN, IMI and ACE. Further studies are necessary to quantify, both experimentally and theoretically, all effects. Specifically, the impact of AChBP environment should be considered so to pave the way towards more rationalised optimisation of the neonicotinoids. Such studies would help to discriminate and quantify precisely the various contributions (specific such as hydrogen-bonding and non specific such as π – π interactions) of the neonicotinoid–nAChR binding process. From an electrophysiological point of view, we find that synaptic and extrasynaptic nAChRs expressed on the sixth abdominal ganglion have not the same sensitivity to DIN, IMI and ACE suggesting that distinct nAChR subtypes are expressed at both synaptic and extrasynaptic receptors. Since it is not possible at the present time to determine the subunit composition of nAChRs expressed on insect due to the difficulty to express functional nAChRs in heterologous systems, our results show that the three neonicotinoids can be separated in two agonist subgroups of various efficiency according to the location of the targeted nAChRs. The first subgroup contains DIN and the second includes IMI and ACE. The coupling of chemical- and biological-based approaches such as the ones used in the present study allows gaining deep insights into the features of neonicotinoids. However, owing to the inherent complexity of insect nAChRs, further work is needed to establish SAR that would help for the design of more potent neonicotinoids.

Aknowledgements

D.J. is indebted to the *Région des Pays de la Loire* for financial support in the framework of a ‘*recrutement sur poste stratégique*’. This work was granted access to the HPC resources of [CCRT/CINES/IDRIS] under the allocation c2011085117 made by GENCI (Grand Equipement National de Calcul Intensif). The authors gratefully acknowledge the CCIPL (Centre de Calcul Intensif des Pays de la Loire) for grants of computer time. We also thank Prof. Tore Brink for allowing access to the most recent version of the HS95 program and for the modifications of the program he has made to allow the calculations of physicochemical properties of the neonicotinoids studied in the present work.

References

- Jeschke, P.; Nauen, R. *Pest Manag. Sci.* **2008**, *64*, 1084.
- Matsuda, K.; Buckingham, S. D.; Kleier, D.; Rauh, J. J.; Grauso, M.; Sattelle, D. B. *Trends Pharmacol. Sci.* **2001**, *22*, 573.
- Shao, X.; Lee, P. W.; Liu, Z.; Xu, X.; Li, Z.; Qian, X. *J. Agric. Food Chem.* **2011**, *59*, 2943.
- Xu, X.; Bao, H.; Shao, X.; Zhang, Y.; Yao, X.; Liu, Z.; Li, Z. *Insect Mol. Biol.* **2010**, *19*, 1.
- Wang, Y.; Cheng, J.; Qian, X.; Li, Z. *Bioorg. Med. Chem.* **2007**, *15*, 2624.
- Jeschke, P.; Nauen, R.; Schindler, M.; Elbert, A. *J. Agric. Food Chem.* **2011**, *59*, 2897.
- Kagabu, S. *J. Agric. Food Chem.* **2011**, *59*, 2887.
- Tomizawa, M.; Casida, J. E. *Annu. Rev. Pharmacol. Toxicol.* **2005**, *45*, 247.
- Tomizawa, M.; Casida, J. E. *Annu. Rev. Entomol.* **2003**, *48*, 339.
- Wells, G. B. *Front Biosci.* **2008**, *13*, 5479.
- Liu, Z.; Williamson, M. S.; Lansdell, S. J.; Denholm, I.; Han, Z.; Millar, N. S. *Proc. Natl. Acad. Sci. U.S.A.* **2005**.
- Liu, Z.; Han, Z.; Zhang, Y.; Song, F.; Yao, X.; Liu, S.; Gu, J.; Millar, N. S. *J. Neurochem.* **2009**, *108*, 498.
- Liu, Z.; Han, Z.; Liu, S.; Zhang, Y.; Song, F.; Yao, X.; Gu, J. *J. Neurochem.* **2008**, *106*, 224.
- Taylor, P.; Talley, T. T.; Radic, Z.; Hansen, S. B.; Hibbs, R. E.; Shi, J. *Biochem. Pharmacol.* **2007**, *74*, 1164.
- Tomizawa, M.; Casida, J. E. *Acc. Chem. Res.* **2009**, *42*, 260.
- Talley, T. T.; Harel, M.; Hibbs, R. E.; Radic, Z.; Tomizawa, M.; Casida, J. E.; Taylor, P. *Proc. Natl. Acad. Sci. U.S.A.* **2008**, *105*, 7606.
- Ihara, M. O. T.; Yamashita, A.; Oda, T.; Hirata, K.; Nishiwaki, H.; Morimoto, T.; Akamatsu, M.; Ashikawa, Y.; Kuroda, S.; Mega, R. K. S.; Sattelle, D. B.; Matsuda, K. *Invertebr. Neurosci.* **2008**, *8*, 71.
- Talley, T. T.; Harel, M.; Hibbs, R. E.; Radic, Z.; Tomizawa, M.; Casida, J. E.; Taylor, P. *Proc. Natl. Acad. Sci. U.S.A.* **2008**, *105*, 7606.
- Ohno, I.; Tomizawa, M.; Durkin, K. A.; Casida, J. E.; Kagabu, S. *J. Agric. Food Chem.* **2009**, *57*, 2436.
- Osztanyi, G.; Suto, A. *Acta Crystallogr., Sect. A* **2004**, *60*, 134.
- Palatinus, L.; Chapuis, G. *J. Appl. Crystallogr.* **2007**, *40*, 786.
- Petricek, V. D. M. JANA2000, a crystallographic computing system: Prague, 2000.
- Allen, F. H. *Acta Crystallogr., Sect. B* **2002**, *58*, 380.
- Macrae, C. F.; Bruno, I. J.; Chisholm, J. A.; Edgington, P. R.; McCabe, P.; Pidcock, E.; Rodriguez-Monge, L.; Taylor, R.; van de Streek, J.; Wood, P. A. *J. Appl. Crystallogr.* **2008**, *41*, 466.
- The Pymol Molecular Graphics System, <http://www.pymol.org>, Delano, W. L.: 2004.
- Gaussian 09, RevA.02; Frisch, M. J. T., G. W.; Schlegel, H. B.; Scuseria, G. E.; Robb, M. A.; Cheeseman, J. R.; Scalmani, G.; Barone, V.; Mennucci, B.; Petersson, G. A.; Nakatsuji, H.; Caricato, M.; Li, X.; Hratchian, H. P.; Izmaylov, A. F.; Bloino, J.; Zheng, G.; Sonnenberg, J. L.; Hada, M.; Ehara, M.; Toyota, K.; Fukuda, R.; Hasegawa, J.; Ishida, M.; Nakajima, T.; Honda, Y.; Kitao, O.; Nakai, H.; Vreven, T.; Montgomery, J. J. A.; Peralta, J. E.; Ogliaro, F.; Bearpark, M.; Heyd, J. J.; Brothers, E.; Kudin, K. N.; Staroverov, V. N.; Kobayashi, R.; Normand, J.; Raghavachari, K.; Rendell, A.; Burant, J. C.; Iyengar, S. S.; Tomasi, J.; Cossi, M.; Rega, N.; Millam, J. M.; Klene, M.; Knox, J. E.; Cross, J. B.; Bakken, V.; Adamo, C.; Jaramillo, J.; Gomperts, R.; Stratmann, R. E.; Yazyev, O.; Austin, A. J.; Cammi, R.; Pomelli, C.; Ochterski, J. W.; Martin, R. L.; Morokuma, K.; Zakrzewski, V. G.; Voth, G. A.; Salvador, P.; Dannenberg, J. J.; Dapprich, S.; Daniels, A. D.; Farkas, O.; Foresman, J. B.; Ortiz, J. V.; Cioslowski, J.; Fox, D. J.: Wallingford CT, 2009.
- Jaguar, 7.8; Schrödinger, L. L. C.: New York, NY, 2011.
- Zhao, Y.; Truhlar, D. G. *J. Phys. Chem. A* **2004**, *108*, 6908.
- van Mourik, T. *J. Chem. Theory Comput.* **2008**, *4*, 1610.
- Jensen, F. *J. Chem. Theory Comput.* **2010**, *6*, 100.
- Reyes, A.; Fomina, L.; Rumsh, L.; Fomine, S. *Int. J. Quantum Chem.* **2005**, *104*, 335.
- Saebo, S.; Tong, W.; Pulay, P. *J. Chem. Phys.* **1993**, *98*, 2170.
- Murray, J. S.; Politzer, P. *J. Chem. Res., Synop.* **1992**, *3*, 110.
- Hagelin, H.; Murray, J. S.; Brinck, T.; Berthelot, M.; Politzer, P. *Can. J. Chem.* **1995**, *73*, 483.
- Murray, J. S.; Ranganathan, S.; Politzer, P. *J. Org. Chem.* **1991**, *56*, 3734.
- Murray, J. S.; Brinck, T.; Grice, M. E.; Politzer, P. *Theochem* **1992**, *88*, 29.
- Brinck, T. *J. Phys. Chem. A* **1997**, *101*, 3408.
- Brinck, T. *Theor. Comput. Chem.* **1998**, *5*, 51.
- Locati, A.; Berthelot, M.; Evain, M.; Lebreton, J.; Le Questel, J.-Y.; Mathe-Allainmat, M.; Planchat, A.; Renault, E.; Graton, J. *J. Phys. Chem. A* **2007**, *111*, 6397.
- Besseau, F.; Graton, J.; Michel, B. *Chem. Eur. J.* **2008**, *14*, 10656.
- Arnaud, V.; Berthelot, M.; Felpin, F.-X.; Lebreton, J.; Le Questel, J.-Y.; Graton, J. *Eur. J. Org. Chem.* **2009**, 4939.
- Kenny, P. W. *J. Chem. Inf. Model.* **2009**, *49*, 1234.
- Bader, R. F. W. *Chem. Rev.* **1991**, *91*, 893.
- Bader, R. F. W. *Atoms in Molecules: A Quantum Theory*; Clarendon: Oxford, 1994.
- Biegler-Koenig, F. W.; Schonbohm, J.; Bayles, D. J. *Comput. Chem.* **2001**, *22*, 545.
- Buckingham, S. D.; Lapiéd, B.; LeCorronc, H.; Grolleau, F.; Sattelle, D. B. *J. Exp. Biol.* **1997**, *200*, 2685.
- Callec, J. J.; Sattelle, D. B. *J. Exp. Biol.* **1973**, *59*, 725.
- Thany, S. H.; Courjaret, R.; Lapiéd, B. *Neurosci. Lett.* **2008**, *438*, 317.
- Thany, S. H. *Neurotoxicology* **2009**, *30*, 1045.
- Kagabu, S.; Matsuno, H. *J. Agric. Food Chem.* **1997**, *45*, 276.
- Sasada, Y. *Chemistry Handbook; The Chemical Society of Japan*; Tokyo: Maruzen, 1984.
- Tomizawa, M.; Zhang, N.; Durkin, K. A.; Olmstead, M. M.; Casida, J. E. *Biochemistry* **2003**, *42*, 7819.
- Kagabu, S.; Ishihara, R.; Hieda, Y.; Nishimura, K.; Naruse, Y. *J. Agric. Food Chem.* **2007**, *55*, 812.
- Chopra, D.; Mohan, T. P.; Rao, K. S.; Row, T. N. G. *Acta Crystallogr., Sect. E* **2004**, *60*, O2415.
- Jeffrey, G. A.; Saenger, W. *Hydrogen Bonding in Biological Structures*; Springer: Berlin, 1991.
- Taylor, R. *Acta Cryst.* **2002**, *D58*, 879.
- Desiraju, G.; Steiner, T. *The Weak Hydrogen Bond: Applications to Structural Chemistry and Biology* **1999**.
- Chopra, D.; Mohan, T. P.; Rao, K. S.; Row, T. N. G. *Acta Cryst.* **2004**, *E60*, O2374.
- Celie, P. H. N.; Van Rossum-Fikkert, S. E.; Van Dijk, W. J.; Breij, K.; Smit, A. B.; Sixma, T. K. *Neuron* **2004**, *41*, 907.
- Hansen, S. B.; Sulzenbacher, G.; Huxford, T.; Marchot, P.; Taylor, P.; Bourne, Y. *EMBO J.* **2005**, *24*, 3635.
- Laurence, C.; Berthelot, M.; Raczynska, E.; Le Questel, J. Y.; Duguay, G.; Hudhomme, P. *J. Chem. Res., Synop.* **1990**, 250.
- Ziao, N.; Laurence, C.; Le Questel, J.-Y. *CrystEngComm* **2002**, *4*, 326.
- Le Questel, J. Y.; Berthelot, M.; Laurence, C. *J. Phys. Org. Chem.* **2000**, *13*, 347.
- Ziao, N.; Graton, J.; Laurence, C.; Le Questel, J. Y. *Acta Cryst.* **2001**, *B57*, 850.
- Allen, F. H.; Baalham, C. A.; Lommerse, J. P. M.; Raithby, P. R.; Sparr, E. *Acta Cryst.* **1997**, *B53*, 1017.
- Steiner, T. *New J. Chem.* **1998**, *22*, 1099.
- Robinson, J. M. A.; Philp, D.; Harris, K. D. M.; Kariuki, B. M. *New J. Chem.* **2000**, *24*, 799.
- Yi, P.-g.; Liu, J.-f.; Song, H.-f. *Jisuanji Yu Yingyong Huaxue* **2000**, *17*, 509.
- Thany, S. H.; Lenaers, G.; Raymond-Delpech, V.; Sattelle, D. B.; Lapiéd, B. *Trends Pharmacol. Sci.* **2007**, *28*, 14.
- Deglise, P.; Grunewald, B.; Gauthier, M. *Neurosci. Lett.* **2002**, *321*, 13.
- Tan, J.; Galligan, J. J.; Hollingworth, R. M. *Neurotoxicology* **2007**, *28*, 829.

72. Thany, S. H. *Neuropharmacology* **2011**, 60, 587.
73. Alix, P.; Grolleau, F.; Hue, B. *J. Neurophysiol.* **2002**, 87, 2972.
74. Miyagi, S.; Komaki, I.; Ozoe, Y. *Pest Manag. Sci.* **2006**, 62, 293.
75. Li, J.; Shao, Y.; Ding, Z.; Bao, H.; Liu, Z.; Han, Z.; Millar, N. S. *Insect Biochem. Mol. Biol.* **2010**, 40, 17.
76. Shao, X.; Lu, H.; Bao, H.; Xu, X.; Liu, Z.; Li, Z. *Insect Biochem. Mol. Biol.* **2011**, 41, 440.